

# Efficiently Luminescent and Stable Lead-free $\text{Cs}_3\text{Cu}_2\text{Cl}_5$ @Silica Nanocrystals for White Light-Emitting Diodes and Communication

Shuangyi Zhao, Chen Chen, Wensi Cai, Ru Li, Haiyun Li, Siqi Jiang, Min Liu, and Zhigang Zang\*

The poor stability of lead-free  $\text{Cs}_3\text{Cu}_2\text{Cl}_5$  nanocrystals (NCs) is the main impediment for their broad practical applications. Here, a sol-gel reaction using tetraethoxysilane (TEOS) as the silica coating precursor to prepare  $\text{Cs}_3\text{Cu}_2\text{Cl}_5$ @ $\text{SiO}_x$  NCs is proposed. Due to the efficient passivation and robust protection of  $\text{SiO}_x$  shells on the NCs surface,  $\text{Cs}_3\text{Cu}_2\text{Cl}_5$ @ $\text{SiO}_x$  NCs solution and films exhibit a high photoluminescence quantum yield of 98% and 76%, respectively, and improved stability against water and heat.  $\text{Cs}_3\text{Cu}_2\text{Cl}_5$ @ $\text{SiO}_x$  NCs are then used to fabricate warm white light-emitting diodes (WLEDs), which show a high color-rendering index of 94 and a proper correlated color temperature of 5049 K, and maintain an excellent thermal (265–360 K) and prolonged operating (380 h) stability. In addition, the good white light emission facilitates the application in visible light communication (VLC). The VLC light source demonstrates a –3 dB bandwidth of 420 kHz, and the achieved data rate of the VLC system reaches 2.65 Mbps using orthogonal frequency division multiplexing modulation with a bit loading. As a result, lead-free  $\text{Cs}_3\text{Cu}_2\text{Cl}_5$ @ $\text{SiO}_x$  NCs with an efficient optical performance and an excellent stability might promote the development of stable NCs and extend the applications in optoelectronics.

employed to replace the toxic Pb. Among the prepared lead-free NCs, 0D  $\text{Cs}_3\text{Cu}_2\text{Cl}_5$  NCs with isolated  $[\text{Cu}_2\text{Cl}_5]^{3-}$  dimers and  $\text{Cs}^+$  ions have recently been reported as a promising material, showing a broad-band green emission and a high photoluminescence yield.<sup>[14–17]</sup> However, the luminescence of  $\text{Cs}_3\text{Cu}_2\text{Cl}_5$  NCs cannot remain in ambient atmosphere due to the oxidation of  $\text{Cu}^+$  to  $\text{Cu}^{2+}$  and the aggregation of NCs.<sup>[18]</sup> Such an instability of  $\text{Cs}_3\text{Cu}_2\text{Cl}_5$  NCs is the main bottleneck for their further commercial applications. Therefore, it is of high urgency to explore an effective route to enhance the stability of  $\text{Cs}_3\text{Cu}_2\text{Cl}_5$  NCs.

Actually, even lead halide perovskite NCs suffer instability issue when exposing to heat, moisture, and water.<sup>[19–21]</sup> One effective strategy to solve such issue is to coat the instable NCs with stable shells, i.e., oxide materials, to protect the NCs against the destruction from heat, moisture and water.<sup>[22–24]</sup> Silica ( $\text{SiO}_x$ ) was reported as an

excellent coating shell due to its transparent characteristic, low cost and excellent stability. Besides, the dense  $\text{SiO}_x$  shell could be prepared by a simple solution method, where the organic silane precursors act as the silica source and hydrolyze into the final silica shells without the addition of excess water.<sup>[25,26]</sup> The obtained lead halide NCs@ $\text{SiO}_x$  show not only an improved stability under heat and water, but also a negligible aggregation, resulting in an increase of photoluminescence quantum yield (PLQY).<sup>[27–31]</sup> As a simple and “waterless” process, the  $\text{SiO}_x$  coating is highly favored and desirable for stabilizing the NCs and enhancing their optical performance.<sup>[32]</sup> Therefore, it is of interest to study whether the unique properties of  $\text{SiO}_x$  coated NCs could be used in lead-free  $\text{Cs}_3\text{Cu}_2\text{Cl}_5$  NCs to improve their luminescent performance and stability.


In this work, we proposed a facile  $\text{SiO}_x$  coating strategy to prepare green-emitting  $\text{Cs}_3\text{Cu}_2\text{Cl}_5$ @ $\text{SiO}_x$  NCs at a low temperature, in which the tetraethoxysilane (TEOS) was chosen as the silane precursor for the formation of  $\text{SiO}_x$  shells. The  $\text{Cs}_3\text{Cu}_2\text{Cl}_5$  NCs were synthesized by a hot-injection method, followed by an addition of TEOS in the as-synthesized NCs at low temperature. Under an optimized amount of TEOS, uniform  $\text{SiO}_x$  shells could be formed on the surface of  $\text{Cs}_3\text{Cu}_2\text{Cl}_5$  NCs, resulting in a negligible aggregation of  $\text{Cs}_3\text{Cu}_2\text{Cl}_5$ -NC film with a high

## 1. Introduction

Lead halide perovskite nanocrystals (NCs) have attracted extensive attention owing to their highly efficient photoluminescence by the quantum confinement effect.<sup>[1,2]</sup> However, the toxicity of lead (Pb) to environment and human body can be a great hindrance for practical applications. To solve such a severe issue, various lead-free elements such as tin (Sn),<sup>[3–5]</sup> copper (Cu),<sup>[6–8]</sup> antimony (Sb),<sup>[9–10]</sup> and bismuth (Bi)<sup>[11–13]</sup> have been

Dr. S. Zhao, Dr. W. Cai, Dr. R. Li, H. Li, S. Jiang, Prof. Z. Zang  
Key Laboratory of Optoelectronic Technology & Systems  
(Ministry of Education)  
Chongqing University  
Chongqing 400044, China  
E-mail: zangzg@cqu.edu.cn

Prof. C. Chen, Prof. M. Liu  
School of Microelectronics and Communication Engineering  
Chongqing University  
Chongqing 400044, China

 The ORCID identification number(s) for the author(s) of this article can be found under <https://doi.org/10.1002/adom.202100307>.

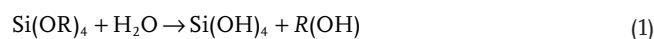
DOI: 10.1002/adom.202100307

PLQY of 76%. Compared with uncoated  $\text{Cs}_3\text{Cu}_2\text{Cl}_5$  NCs, coated NCs exhibit an excellent stability against heat and water, owing to the protection by the formed  $\text{SiO}_x$  shells. Warm white light-emitting diodes (WLEDs) were also fabricated by mixing the stable and efficiently luminescent  $\text{Cs}_3\text{Cu}_2\text{Cl}_5@ \text{SiO}_x$  NCs with red-emitting phosphors. Owing to the high PLQY and broad-band emission of  $\text{Cs}_3\text{Cu}_2\text{Cl}_5@ \text{SiO}_x$  NCs, the WLEDs show a high color rendering index (CRI) of 94 and an appropriate correlated color temperature (CCT) of 5049 K. Such WLEDs also maintain well-operated under various temperatures between 265 and 360 K, with an excellent operating stability of  $\approx 380$  h. In addition, the high-performance WLEDs were employed as light sources in visible light communication (VLC), showing  $-3$  dB bandwidth of 420 kHz and an achievable data rate of 2.65 Mbps using orthogonal frequency division multiplexing (OFDM) modulation with a bit loading, suggesting their potential applications in VLC. Therefore, this work demonstrates the promising potential of stable lead-free  $\text{Cs}_3\text{Cu}_2\text{Cl}_5@ \text{SiO}_x$  NCs in both white-light diodes and communications, which may possess great opportunities in harsh conditions and the other novel fields.

## 2. Results and Discussion

In this work, a two-step method was used to prepare  $\text{Cs}_3\text{Cu}_2\text{Cl}_5$  NCs and coat the surface of the NCs with  $\text{SiO}_x$ . The synthesis procedures are illustrated in Figure 1a.  $\text{Cs}_3\text{Cu}_2\text{Cl}_5$  NCs were

prepared by a hot-injection method followed by the adding of the as-prepared NCs solutions with various amount of the tetraethoxysilane (TEOS), in which the TEOS acts as the silane precursor. Among the various silica precursors, TEOS is regarded as a good silica precursor for  $\text{Cs}_3\text{Cu}_2\text{Cl}_5$  NCs because of its proper hydrolysis rate and chemical stability. The proper hydrolysis rate enables the formation of a silica shell on single nanocrystal without aggregation and additional water. To decrease the hydrolysis reaction time, the mixture of NCs and TEOS was stirred at  $50^\circ\text{C}$  to enable to the formation of  $\text{SiO}_x$  shells. The stirring mixture was exposed to air with the trace of water vapor being captured and reacted with TEOS for its hydrolysis to  $\text{SiO}_x$ , as represented by the follow reactions:<sup>[25]</sup>



As shown in Figure 1b,  $\text{Cs}_3\text{Cu}_2\text{Cl}_5$  NCs exhibits a direct bandgap of 3.72 eV at the  $\Gamma$  point, which is agreement with the values reported previously.<sup>[17]</sup> Besides, a flat valance band maximum (VBM) is found, indicating strong excitons location and heavy hole effective mass and are the characteristic of 0D  $\text{Cs}_3\text{Cu}_2\text{Cl}_5$  NCs. As shown in Figure 1c, the PDOS (projected density of states) results show that the VBM is contributed mostly by Cu 4s and Cl 3p orbits, whereas the conduction band minimum (CBM) is mainly contributed by the hybrid orbits of Cu 3d and Cl 3p.<sup>[33–36]</sup>

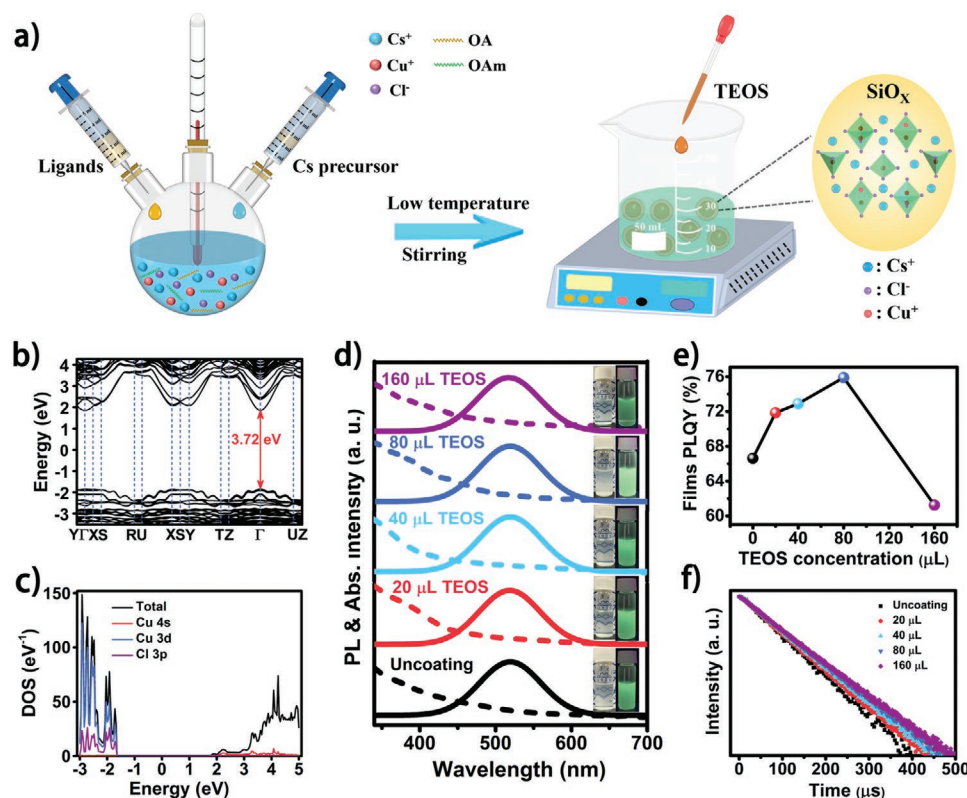


**Figure 1.** a) Reaction process of the coating of  $\text{Cs}_3\text{Cu}_2\text{Cl}_5@ \text{SiO}_x$  NCs. b) Electronic band structure and c) PDOS results of  $\text{Cs}_3\text{Cu}_2\text{Cl}_5$  NCs. d) PL and absorption spectra of uncoated  $\text{Cs}_3\text{Cu}_2\text{Cl}_5$  NCs and  $\text{Cs}_3\text{Cu}_2\text{Cl}_5@ \text{SiO}_x$  NCs with various amounts of TEOS. e) Room-temperature PLQY and f) PL decay curves of uncoated  $\text{Cs}_3\text{Cu}_2\text{Cl}_5$ -NC and  $\text{Cs}_3\text{Cu}_2\text{Cl}_5@ \text{SiO}_x$ -NC films with various amounts of TEOS.

The photoluminescence and absorption spectra of uncoated and coated  $\text{Cs}_3\text{Cu}_2\text{Cl}_5$  NCs are shown in Figure 1d. It is found that the  $\text{SiO}_x$  coating does not affect the location of emissive peaks (locate at 523 nm). Also, negligible changes are found for the absorption results of  $\text{Cs}_3\text{Cu}_2\text{Cl}_5@ \text{SiO}_x$  NCs with the adding of various amounts of TEOS. However, it is obvious that the variety of TEOS amounts affects the emissive intensity of NCs, as confirmed by the inset of Figure 1d.  $\text{Cs}_3\text{Cu}_2\text{Cl}_5$  NCs generally exhibit unique optical properties, including a broad PL emission and large Stokes shifts arising from self-trapped excitons (STEs).<sup>[37,38]</sup> Since no change of PL and absorption peaks is found after the coating with  $\text{SiO}_x$ , the coating should not affect the formation of STEs. The good transparency and chemical stability also suggest that  $\text{SiO}_x$  is an excellent candidate for the coating of NCs. In fact, the STEs are decided from the electronic band structure of  $\text{Cs}_3\text{Cu}_2\text{Cl}_5$  NCs, which can be calculated from the results of density functional theory (DFT). The negligible oxidation of  $\text{Cu}^+$  in Figure 1b,c suggests a maintained electronic band structure, which might be responsible for the unchanged PL and absorption spectra of coating NCs.

The adding of TEOS results in an increase of PLQY, showing a highest of  $\approx 76\%$  for  $\text{Cs}_3\text{Cu}_2\text{Cl}_5@ \text{SiO}_x$ -NC films with the adding of 80  $\mu\text{L}$  TEOS (Figure 1e), whereas the PLQY of the corresponding NC solution reaches  $\approx 98\%$ . It was previously reported that the surface defects of NCs might quench the emission performance.<sup>[39,40]</sup> Therefore, the enhancement of the PLQY is considered mainly due to the reduction of surface defects by the effective passivation using  $\text{SiO}_x$ . With the increase of TEOS amounts, uniform and dense  $\text{SiO}_x$  shells may form on the surface of NCs to passivate the surface defects, leading to the increase of radiative recombination. However, the introduction of excess TEOS (160  $\mu\text{L}$ ) results in a decrease of PLQY for the NCs film, possibly due to the destruction of NCs by the large production of water during the TEOS hydrolysis. As described in Equation (1) and (2), the water which is absorbed from air may be produced and released to the final production. The large amounts of TEOS precursors can absorb more water from air and release more water into the coating  $\text{Cs}_3\text{Cu}_2\text{Cl}_5$  NCs, leading to the destruction of NCs. To investigate the enhancement of PLQY with proper amounts of  $\text{SiO}_x$  coating, PL decay was measured to study the radiative recombination, as shown in Figure 1f. The PL lifetime decay curves are fitted by a biexponential function, in which the fast decay time ( $\tau_1$ ) and slow decay time ( $\tau_2$ ) are the radiative recombination of the excitons and the nonradiative recombination induced by the surface defects, respectively. The fitting results are summarized in Table 1. It is found that  $\tau_1$  and  $\tau_2$  increase from

75.2/118.9 to 96.2/143.7  $\mu\text{s}$  with the increase of TEOS amount to 160  $\mu\text{L}$ . Apart from the increase of decay time, the ratios of  $A_1/A_2$  also increase with the introduction of  $\text{SiO}_x$  shells, indicating an improved radiative recombination and a dominant of  $\text{Cs}_3\text{Cu}_2\text{Cl}_5@ \text{SiO}_x$  NCs by the radiative recombination of the excitons.<sup>[41]</sup>

The amounts of the TEOS play a crucial role in the optical performance of  $\text{Cs}_3\text{Cu}_2\text{Cl}_5@ \text{SiO}_x$  shells. To study it, transmission electron microscopy (TEM) was performed for  $\text{Cs}_3\text{Cu}_2\text{Cl}_5$  NCs coated with different amounts of TEOS, as shown in Figure 2. Both uncoated and coated  $\text{Cs}_3\text{Cu}_2\text{Cl}_5$  NCs show a crystalline structure, as evidenced by the selected-area electron diffraction images (the inset of Figure 2a–e). Uncoated  $\text{Cs}_3\text{Cu}_2\text{Cl}_5$  NCs show a sphere morphology with a mean size of  $\approx 4.6$  nm (Figure 2a and Figure S1a, Supporting Information), and the coating of silica does not change the sphere-like nanostructure of  $\text{Cs}_3\text{Cu}_2\text{Cl}_5$  NCs (Figure 2b,e). However, the high-resolution TEM (HRTEM) images show that the amounts of added TEOS affect the formation and uniformity of  $\text{SiO}_x$  shells. Specifically, when adding 20 or 40  $\mu\text{L}$  TEOS, the corresponding  $\text{SiO}_x$  shells are thin and nonuniform, with the size distribution results showing a slight increase in size and a dispersive size distribution (Figure S1b,c, Supporting Information), suggesting that these amounts of TEOS (20 and 40  $\mu\text{L}$ ) are not able to form dense and uniform  $\text{SiO}_x$  shells. While when 80  $\mu\text{L}$  TEOS are added to coat  $\text{Cs}_3\text{Cu}_2\text{Cl}_5$  NCs, both TEM and HRTEM (Figure 2d), images illustrate the formation of uniform  $\text{SiO}_x$  shells on the surface of NCs with an increased size ( $\approx 5.1$  nm) owing to the thickness of  $\text{SiO}_x$  shells ( $\approx 0.25$  nm, Figure S1d, Supporting Information). Since the coating of  $\text{SiO}_x$  has negligible effect on the dispersion and crystallinity, the favor of  $\text{SiO}_x$  on the coating of nanocrystals is demonstrated. However, when 160  $\mu\text{L}$  TEOS are added to coat the NCs, the excessive TEOS may hydrolyze to be a gel matrix to wrap the  $\text{Cs}_3\text{Cu}_2\text{Cl}_5$  NCs, leading to the aggregation of NCs, as shown in Figure 2e. Figure 2f,g and Figure S2 (Supporting Information) show the elements mapping and energy-dispersive spectroscopy (EDS) analysis results of the  $\text{Cs}_3\text{Cu}_2\text{Cl}_5$  NCs and  $\text{Cs}_3\text{Cu}_2\text{Cl}_5@ \text{SiO}_x$  NCs with 80 and 160  $\mu\text{L}$  TEOS, respectively. The existence of cesium (Cs), copper (Cu), chlorine (Cl), silicon (Si), and oxygen (O) elements demonstrates the successful coating of  $\text{SiO}_x$  on the  $\text{Cs}_3\text{Cu}_2\text{Cl}_5$  NCs and suggests that the coating process cannot decompose the  $\text{Cs}_3\text{Cu}_2\text{Cl}_5$  NCs.

To further study the crystallinity of  $\text{Cs}_3\text{Cu}_2\text{Cl}_5$  NCs induced by the coating of  $\text{SiO}_x$ , X-ray diffraction (XRD) characterizations of the uncoated and coated  $\text{Cs}_3\text{Cu}_2\text{Cl}_5$  NCs with various amounts of TEOS were performed. As shown in Figure 3a, the XRD results of the coated  $\text{Cs}_3\text{Cu}_2\text{Cl}_5$  NCs display a satisfied consistence with the standard  $\text{Cs}_3\text{Cu}_2\text{Cl}_5$  NCs diffraction, suggesting that the  $\text{SiO}_x$  coating may not affect the crystallinity and phase of original  $\text{Cs}_3\text{Cu}_2\text{Cl}_5$  NCs, in agreement with the TEM and HRTEM results. In addition, while the uncoated  $\text{Cs}_3\text{Cu}_2\text{Cl}_5$  NCs show small diffraction peaks of  $\text{Cs}_2\text{CuCl}_4$ ,  $\text{Cs}_3\text{Cu}_2\text{Cl}_5@ \text{SiO}_x$  NCs exhibit only the diffraction features of  $\text{Cs}_3\text{Cu}_2\text{Cl}_5$  NCs, indicating that the coating with  $\text{SiO}_x$  shells indeed protects the NCs against oxidation. The surface functional groups of uncoated and coated  $\text{Cs}_3\text{Cu}_2\text{Cl}_5$  NCs have been characterized using Fourier transform infrared spectroscopy (FTIR), as shown in Figure 3b. Strong Si-O-Si peaks at the 750, 1022, and

**Table 1.** PL decay times of  $\text{Cs}_3\text{Cu}_2\text{Cl}_5$ -NC films coated with various amounts of TEOS.

TEOS amount [ $\mu\text{L}$ ]	$\tau_1$ [ $\mu\text{s}$ ]	$\tau_2$ [ $\mu\text{s}$ ]	$A_1$ [%]	$A_2$ [%]	PLQY [%]
0	75.2	118.9	22.9	77.1	66.9
20	85.6	122.7	36.1	63.9	71.4
40	89.1	128.7	38.3	61.7	72.7
80	94.6	137.5	64.4	35.6	75.9
160	96.2	143.7	71.0	29.0	61.5



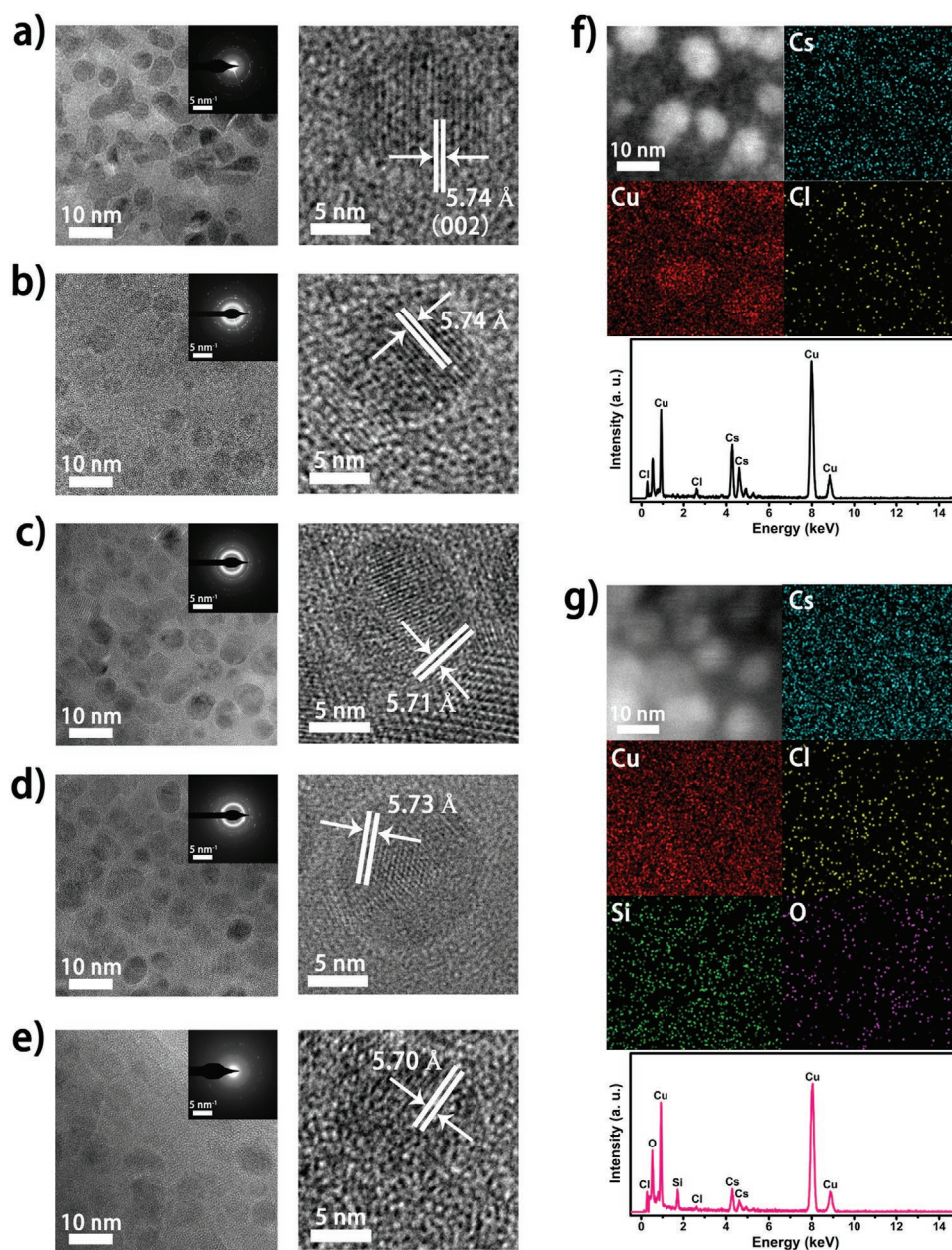


**Figure 2.** Transmission electron microscopy (TEM) (left) and high-resolution TEM (HRTEM) images of a) uncoated Cs<sub>3</sub>Cu<sub>2</sub>Cl<sub>5</sub> NCs and of Cs<sub>3</sub>Cu<sub>2</sub>Cl<sub>5</sub>@SiO<sub>x</sub> NCs synthesized with b) 20 μL, c) 40 μL, d) 80 μL, and e) 160 μL TEOS, respectively. f) Cesium (Cs), copper (Cu), and chlorine (Cl) elemental mapping images and EDS (energy dispersive spectrometer) of uncoated Cs<sub>3</sub>Cu<sub>2</sub>Cl<sub>5</sub> NCs. g) Cs, Cu, Cl, Si, O elemental mapping images and EDS results of Cs<sub>3</sub>Cu<sub>2</sub>Cl<sub>5</sub>@SiO<sub>x</sub> NCs synthesized with 80 μL TEOS.

1108 cm<sup>-2</sup> are found, confirming the formation of the SiO<sub>x</sub>. The peaks at 2923 and 2854 cm<sup>-1</sup> in Cs<sub>3</sub>Cu<sub>2</sub>Cl<sub>5</sub>@SiO<sub>x</sub> NCs can be ascribed to the asymmetric and symmetric stretching vibrations of C–H bonds, which come from the oleic acid (OA) and oleylamine (OAm) ligands on the surface of NCs.<sup>[26]</sup> The presence of C–H bonds in the Cs<sub>3</sub>Cu<sub>2</sub>Cl<sub>5</sub>@SiO<sub>x</sub> suggests that the coating of SiO<sub>x</sub> can maintain the ligands on the surface of NCs and prevents them from dropping.

X-ray photoelectron spectroscopy (XPS) was also performed to evaluate the elements states, as shown in Figure 3c. While peaks for Cs, Cu, and Cl can be observed in both NCs, the

strong peaks of Si and O only appear in Cs<sub>3</sub>Cu<sub>2</sub>Cl<sub>5</sub>@SiO<sub>x</sub> NCs. As shown in Figure 3d, the negligible peaks for Cu<sup>2+</sup> in Cs<sub>3</sub>Cu<sub>2</sub>Cl<sub>5</sub>@SiO<sub>x</sub> NCs demonstrate the protective effect of SiO<sub>x</sub> shells against oxidation of Cu<sup>+</sup> to Cu<sup>2+</sup>.<sup>[42,43]</sup> The existence of Si in the Cs<sub>3</sub>Cu<sub>2</sub>Cl<sub>5</sub>@SiO<sub>x</sub> NCs further confirms the presence of the SiO<sub>x</sub> shells on the surface of NCs (Figure 3e). As shown in Figure S3 (Supporting Information), the shifts of O peaks are found in both NCs, which are resulted from the different chemical states of oxygen elements. For uncoated Cs<sub>3</sub>Cu<sub>2</sub>Cl<sub>5</sub> NCs, the oxygen element originates from the oxidation of NCs, which corresponds to a valence state of –2. This is different

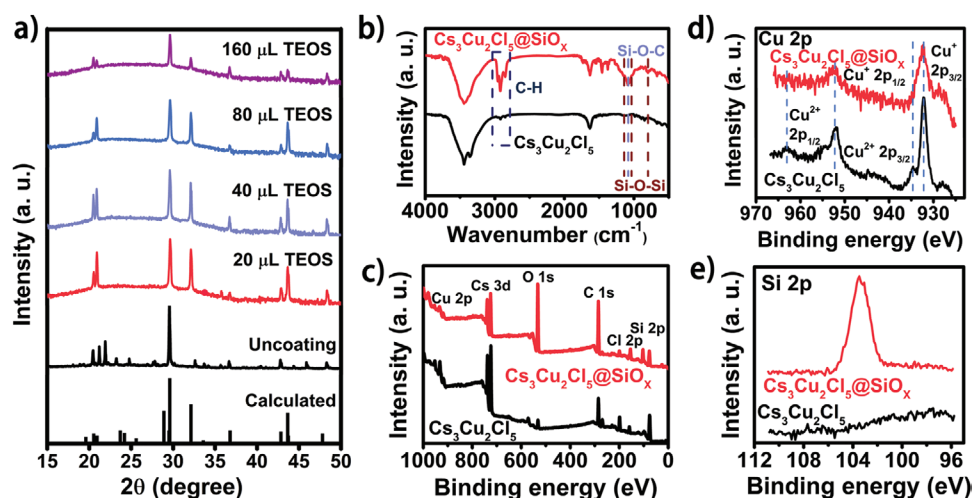


**Figure 3.** a) XRD patterns of  $\text{Cs}_3\text{Cu}_2\text{Cl}_5$  NCs and  $\text{Cs}_3\text{Cu}_2\text{Cl}_5@\text{SiO}_x$  NCs synthesized with various amounts of TEOS, respectively. b) FTIR spectra and c) XPS spectra of uncoated  $\text{Cs}_3\text{Cu}_2\text{Cl}_5$  NCs and  $\text{Cs}_3\text{Cu}_2\text{Cl}_5@\text{SiO}_x$  NCs. XPS element analysis of d) Cu 2p and e) Si 2p of uncoated  $\text{Cs}_3\text{Cu}_2\text{Cl}_5$  NCs and  $\text{Cs}_3\text{Cu}_2\text{Cl}_5@\text{SiO}_x$  NCs.

from the case of  $\text{Cs}_3\text{Cu}_2\text{Cl}_5@\text{SiO}_x$ , as the oxidation of Cu element is negligible. The O state here may originate from the  $\text{SiO}_x$  shells. Hence, the shift of O state can be ascribed to the nonstoichiometry of  $\text{SiO}_x$ , where the O state doesn't correspond to an absolute valence state of  $-2$  and the silica shells should be considered as amorphous  $\text{SiO}_x$ .

In addition to the improvement of the optical performance induced by the silica coating, the change of stability of the  $\text{Cs}_3\text{Cu}_2\text{Cl}_5@\text{SiO}_x$  NCs was investigated. For uncoated  $\text{Cs}_3\text{Cu}_2\text{Cl}_5$  NCs, the water and moisture may accelerate the oxidation of  $\text{Cu}^+$  ions and the decomposition of  $\text{Cs}_3\text{Cu}_2\text{Cl}_5$ . Also, owing to the low binding energy of ligands on the NCs, the surface ligands may easily drop from the NCs when the NCs are processed in a thermal treatment, leading to the aggregation of NCs, and resulting in a decreased emission and stability. However, by coating the  $\text{Cs}_3\text{Cu}_2\text{Cl}_5$  NCs with uniform and dense  $\text{SiO}_x$  shells, the oxidation and aggregation can be prevented. Here, the stability of  $\text{Cs}_3\text{Cu}_2\text{Cl}_5$  NCs and  $\text{Cs}_3\text{Cu}_2\text{Cl}_5@\text{SiO}_x$  NCs under heating and against water were evaluated. **Figure 4a–c** shows the PL intensity evolution of  $\text{Cs}_3\text{Cu}_2\text{Cl}_5$  NCs and  $\text{Cs}_3\text{Cu}_2\text{Cl}_5@\text{SiO}_x$  NCs under a continuous heating of  $80^\circ\text{C}$ . The PL intensity of uncoated NCs reduces to 10% of their initial value after 18 days, while it maintains 57% of the initial for  $\text{Cs}_3\text{Cu}_2\text{Cl}_5@\text{SiO}_x$ . Similarly, the stability against water also enhanced after the  $\text{SiO}_x$  coating. When adding water into the NCs solution, the PL intensity of  $\text{Cs}_3\text{Cu}_2\text{Cl}_5@\text{SiO}_x$  NCs maintains 55% of their initial PL intensity after 100 minutes while only 17% of the initial remains for uncoated NCs even after 60 min, as shown in **Figure 4d–f**. To further study the improved stability induced by the  $\text{SiO}_x$  coating, the final products in the stability tests were characterized using XRD (**Figure S4**, Supporting Information), which shows diffraction peaks of  $\text{Cs}_2\text{CuCl}_4$ ,  $\text{CsCl}$  and  $\text{CuCl}_2$  after treatments with heat and water. The existence of  $\text{Cs}_2\text{CuCl}_4$  is considered mainly due to the oxidation while the presence of  $\text{CsCl}$  and  $\text{CuCl}_2$  might be ascribed to the decomposition. It implies that the oxidation is regarded as the major reason for PL quenching of  $\text{Cs}_3\text{Cu}_2\text{Cl}_5$  NCs, whereas the decomposition and oxidation are responsible to the reduction of their optical performance. As a comparison,

owing to the protective effect of the  $\text{SiO}_x$  shells, the oxidation and decomposition are suppressed in  $\text{Cs}_3\text{Cu}_2\text{Cl}_5@\text{SiO}_x$  NCs, resulting in a significantly enhanced stability. Furthermore, we study the thermal stability of the uncoated and coated  $\text{Cs}_3\text{Cu}_2\text{Cl}_5$  NCs at a higher temperature using the TGA (thermogravimetric analysis). As shown in **Figure S5** (Supporting Information), a slight weight loss at  $200\text{--}500^\circ\text{C}$  is expected to be attributed to the thermal decomposition of unreacted silica precursors. The  $\text{Cs}_3\text{Cu}_2\text{Cl}_5$  NCs are observed to decompose at  $\approx 510^\circ\text{C}$ , whereas the decomposing temperature of  $\text{Cs}_3\text{Cu}_2\text{Cl}_5@\text{SiO}_x$  NCs is  $\approx 580^\circ\text{C}$ , revealing the enhanced thermal stability induced from silica coating and suggesting a slower decomposing speed of  $\text{Cs}_3\text{Cu}_2\text{Cl}_5@\text{SiO}_x$  NCs. After the thermal decomposition,  $\approx 20\%$  residual was observed in  $\text{Cs}_3\text{Cu}_2\text{Cl}_5@\text{SiO}_x$  NCs, which is due to the existence of silica in the  $\text{Cs}_3\text{Cu}_2\text{Cl}_5@\text{SiO}_x$  NCs since silica show a high boiling point of  $>1200^\circ\text{C}$ . The results therefore demonstrate the significant effect of silica coating on enhancement of thermal stability of NCs.

To demonstrate the potential optoelectronic applications of lead-free  $\text{Cs}_3\text{Cu}_2\text{Cl}_5@\text{SiO}_x$  NCs, the warm white light-emitting diodes (WLEDs) are fabricated by depositing the coated NCs and commercial red  $\text{CaAlSiN}_3:\text{Eu}^{2+}$  phosphors on UV excitation chips. **Figure 5a** displays a series of electroluminescence (EL) spectra of WLEDs with increasing driving voltages. All EL spectra demonstrate two clear peaks at 523 and 660 nm, which are the emission of  $\text{Cs}_3\text{Cu}_2\text{Cl}_5@\text{SiO}_x$  NCs and  $\text{CaAlSiN}_3:\text{Eu}^{2+}$  phosphors, respectively. With the increase of driving voltages from 4.6 to  $4.8\text{ V}$ , the EL intensity of entire spectra enhances gradually, as shown in **Figure S6** (Supporting Information). **Figure 5b** shows photographs of as-prepared WLEDs operated both under daylight and in dark. It is found that the emission of WLEDs is warm white light, which is harmless for naked eyes of human. Moreover, the WLEDs exhibit an excellent emissive performance with a CIE color coordinate of (0.346, 0.378) (**Figure 5c**), a high color rendering index (CRI) of 94 and a proper correlated color temperature (CCT) of 5049 K. These features are very close to those of sunlight, implying the promising potential of our WLEDs in illumination.



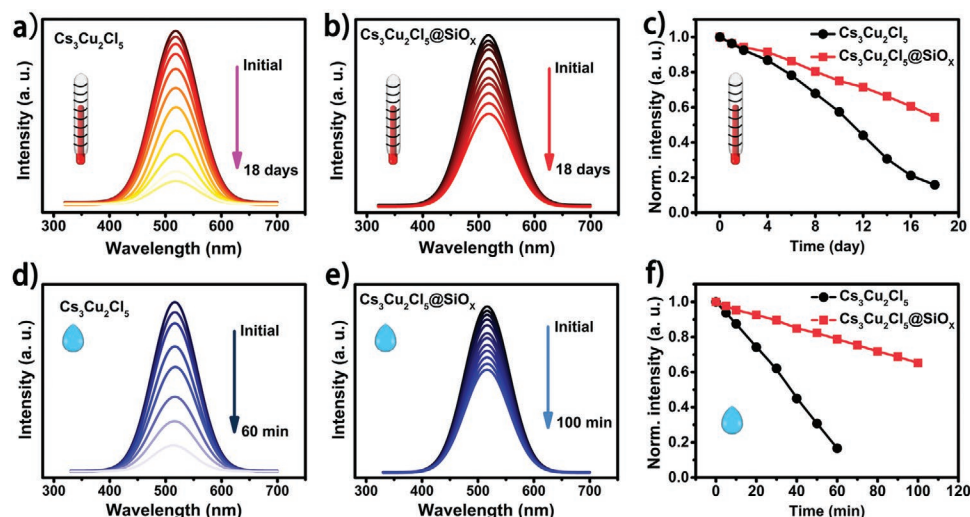


**Figure 4.** a,b) PL spectra and c) normalized PL intensity of uncoated  $\text{Cs}_3\text{Cu}_2\text{Cl}_5$  NCs and  $\text{Cs}_3\text{Cu}_2\text{Cl}_5@\text{SiO}_x$  NCs with 80  $\mu\text{L}$  TEOS during a heat treatment at 80 °C. d,e) PL spectra and f) normalized PL intensity of uncoated  $\text{Cs}_3\text{Cu}_2\text{Cl}_5$  NCs and  $\text{Cs}_3\text{Cu}_2\text{Cl}_5@\text{SiO}_x$  NCs with 80  $\mu\text{L}$  TEOS measured with adding of water.

In addition, the stability of the WLEDs at various temperatures and under a prolonged operation were studied. Figure 5d shows the EL spectra of WLEDs operating at various temperatures from 265 to 360 K, presenting a negligible shift of EL spectra during the temperature test. As shown in Figure 5e,f, small changes of power efficiency as well as CRI and CCT values occur, which are due to the variety of emissive

intensity of the  $\text{Cs}_3\text{Cu}_2\text{Cl}_5@\text{SiO}_x$  NCs, as shown in Figure S7a (Supporting Information). With the increase of temperature, the emissive intensity of NCs first increases and then reduces. The increase and reduction of emissive intensity is owing to the thermal excitation and thermal quenching, respectively, but the thermal effects on the optical performance of WLEDs is found to be small. Thus, the CIE color coordinates of WLEDs during

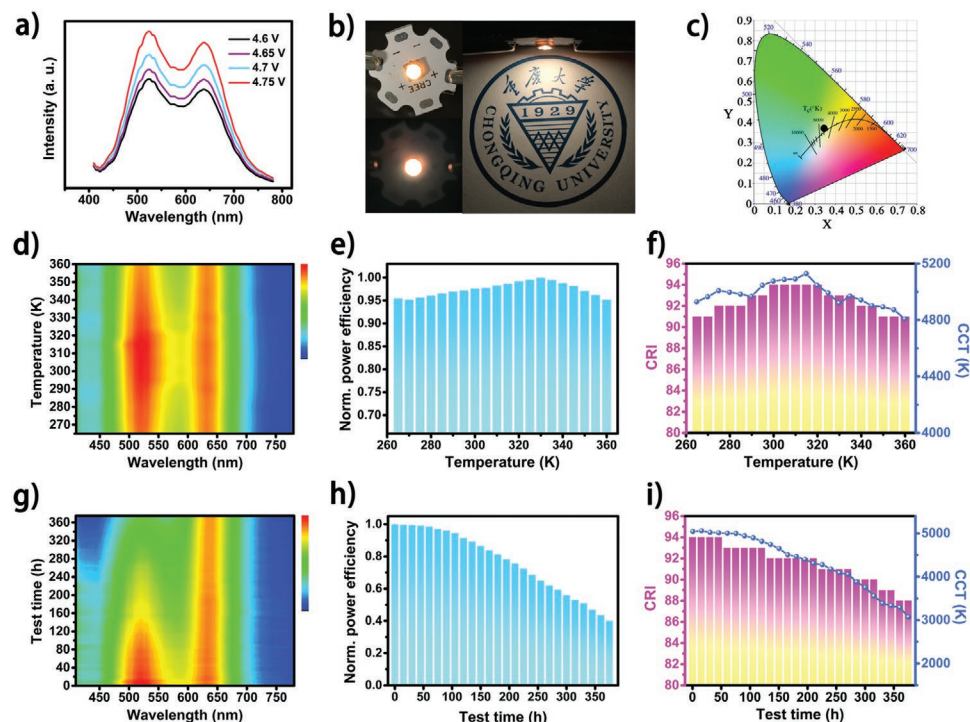


**Figure 5.** a) EL spectra of as-prepared white light-emitting diodes (WLEDs) with green  $\text{Cs}_3\text{Cu}_2\text{Cl}_5@\text{SiO}_x$  NCs and red phosphors. b) Photographs of the emissive WLEDs obtained in dark and under daylight. c) CIE chromaticity diagram of the WLEDs. d) Pseudocolor plot of the EL spectra; evolution of e) the normalized power efficiency and f) CRI and CCT of WLEDs measured at various temperatures. g) Pseudocolor plot of the EL spectra; evolution of h) the normalized power efficiency and i) CRI and CCT of WLEDs during an operation of 380 h.

the thermal test may vary in a small range (Figure S7b, Supporting Information), resulting in a negligible change of the DUV values, as shown in Figure S7c (Supporting Information). Furthermore, the WLEDs were tested for a prolonged operating time of 380 h, and the EL results are shown in Figure 5g. It is found that the red peaks maintain but the green peaks, corresponding to the emission of  $\text{Cs}_3\text{Cu}_2\text{Cl}_5/\text{SiO}_x$  NCs, decrease to only 50% of their initial intensity after 380-hour operation at a driving voltage of 4.7 V (Figure S8a, Supporting Information), confirming the excellent operating stability of WLEDs. Figure 5h,i shows that although the power efficiency as well as CRI and CCT values decrease with the increase of test time, WLEDs exhibit a  $\approx 40\%$  power efficiency of initial value, a high CRI value of 88 and a proper CCT of 3069 K after an continuous operation of 380 h, due to the good chemical stability of  $\text{Cs}_3\text{Cu}_2\text{Cl}_5/\text{SiO}_x$  NCs. Figure S8b (Supporting Information) shows the CIE color coordinates of WLEDs shift due to the changes of EL spectra, with the DUV values observed to vary in the range of 0.0098 to  $-0.0041$ , as shown in Figure S8c (Supporting Information), suggesting the potential as illumination sources with a long-time operation.

The fabricated WLEDs were also used as the optical sources for visible light communication (VLC), which serves the dual-function of simultaneous lighting and communication, as shown in Figure 6a. Figure 6b shows the measured electrical-optical-electrical (EOE) frequency response of the VLC system using the fabricated WLEDs with a DC bias of 7.0 V. The measured EOE frequency response exhibits a typical low-pass characteristic with an obtained  $-3$  dB bandwidth of about 420 kHz.

The received signal-to-noise ratio (SNR) of the VLC system is shown in Figure 6c, from which a gradually decreased SNR value with the increase of frequency is clearly observed. To fully explore the achievable transmission data rate of the VLC system using the fabricated WLEDs, the orthogonal frequency division multiplexing (OFDM) modulation with a bit loading is applied according to the measured SNR performance, as shown in Figure 6c. The resultant bit loading profile is plotted in Figure 6d and the corresponding received constellation diagrams, including binary phase shift keying (BPSK), 4-ary quadrature amplitude modulation (4QAM), 8QAM and 16QAM, are shown in Figure 6e. Using OFDM modulation with a bit loading, the achieved data rate of the VLC system using the fabricated WLED is about 2.65 Mbps, which is more than six times of the measured  $-3$  dB bandwidth.

### 3. Conclusion

In summary, we reported a facile two-step solution method to coat the lead-free  $\text{Cs}_3\text{Cu}_2\text{Cl}_5$  NCs films with  $\text{SiO}_x$  shells at a low temperature, which resulted in an enhanced PL performance with a high PLQY of 76% and an improved stability against water, moisture and heat. The effective surface passivation using  $\text{SiO}_x$  shells is considered as the main reason for the performance enhancement, which suppresses the surface defects of NCs and eliminates the aggregation. WLEDs based on the optimum  $\text{Cs}_3\text{Cu}_2\text{Cl}_5/\text{SiO}_x$  NCs show high CRI values of 94 and proper CCT of 5049 K, as well as a low DUV of 0.0097.

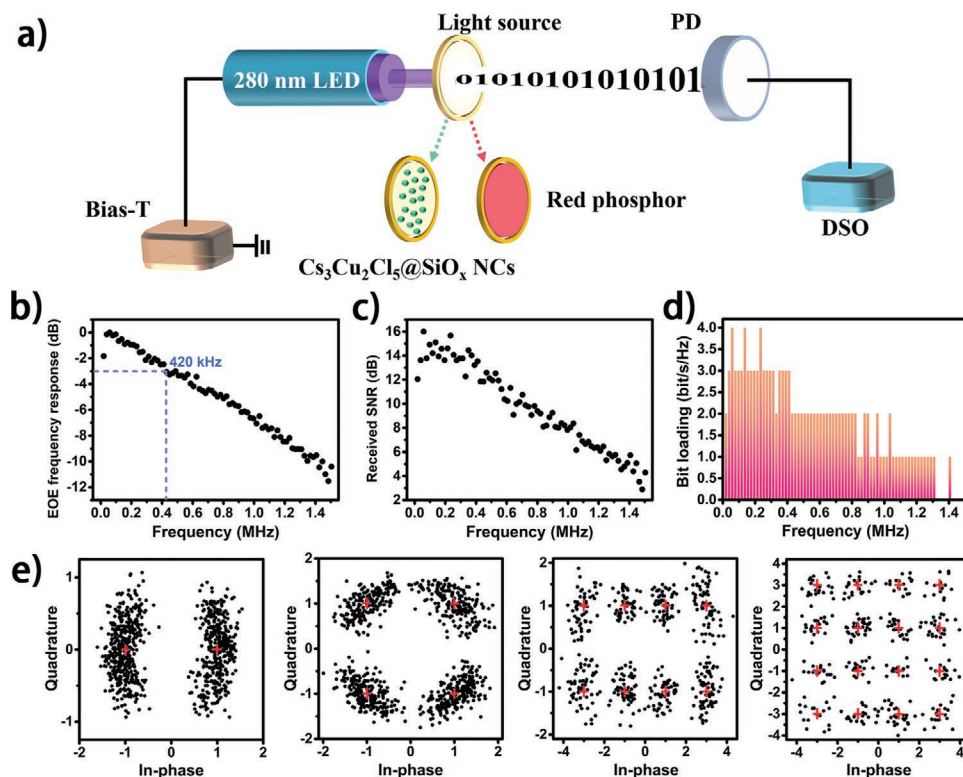


**Figure 6.** a) Schematic diagrams of the VLC system. b) EOE frequency response, c) received SNR, d) bit loading profile of the WLEDs as light sources in the VLC system, and e) the corresponding constellation diagrams of BPSK, 4QAM, 8QAM, and 16QAM.

The WLEDs also exhibit an excellent stability under high temperature and a long-term stability over a continuous operation for 380-hour owing to reduced oxidation and decomposition by the robust and protective  $\text{SiO}_x$  shells. In addition, the fabricated WLEDs were utilized in white light communication, which displayed a  $-3\text{ dB}$  bandwidth of 420 kHz and an achievable data rate of 2.65 Mbps using OFDM modulation with a bit loading. The excellent optical performance and water/heat resistance of the fabricated lead-free NCs can extend their application fields, such as medical diagnosis, bio-imaging, indoor illumination, solar simulator and Internet of Things (IoT). The reported simple coating method might be also applicable for other unstable NCs because of its facility and universality in enhancement of performance and improvement of stability.

## 4. Experimental Section

**Materials:** Cesium carbonate ( $\text{Cs}_2\text{CO}_3$ , 99.9%) was purchased from Xi'an polymer Light Technology Corp. Copper (monovalence) chloride ( $\text{CuCl}$ , 99.9%) was purchased from Macklin Inc. Octadecene (ODE, >90%), Oleic acid (OA, >90%), and Oleylamine (OAm, >90%) were purchased from Adamas. Tetraethoxysilane (TEOS) was purchased from Aladdin Bio-Chem Technology Co., LTD. Toluene and *n*-hexane were purchased from Sinopharm Inc. All these reagents were used without any further purification.

**Synthesis of  $\text{Cs}_3\text{Cu}_2\text{Cl}_5$  Nanocrystals (NCs):** 305 mg  $\text{Cs}_2\text{CO}_3$ , 15 mL ODE, and 1 mL OA were loaded into a 100 mL three-neck flask to prepare the Cs-precursor. 39.6 mg  $\text{CuCl}$  and 10 mL ODE were loaded into another 100 mL three-neck flask. The two flasks were firstly degassed for 15 min. Then both flasks were heated to 120 °C, followed by a quick adding of 0.5 mL OA and 0.5 mL OAm into the Cu-flask at 120 °C under nitrogen flow. After  $\text{CuCl}$  powders were completely dissolved, the reaction temperature was maintained at 120 °C for 10 min. Finally, 3 mL Cs-precursor was quickly injected into the Cu-flask and the mixture was cooled in an ice–water bath to room temperature after 5 s. To obtain NCs with a small size, the Cu-flask with final production should be cooled in an ice bath for at least 1 min to quench the growth of NCs. The as-prepared crude NCs solution were used in next process without any wash and purification.

**$\text{SiO}_x$  Coating of  $\text{Cs}_3\text{Cu}_2\text{Cl}_5$  NCs:** 4 mL as-prepared  $\text{Cs}_3\text{Cu}_2\text{Cl}_5$  NCs solution was loaded in a 10 mL bottle, followed by the adding of various amounts of TEOS. The bottles with NCs and TEOS were open to air and the mixed solution was stirred on a hot plate at 50 °C until lots of white precipitations being observed in the bottom of the bottles, which correspond to the  $\text{SiO}_x$  with size of micrometers. The supernatant in the bottles was collected and centrifuged at 9000 rpm for 8 min. After centrifugation, the supernatant was discarded and the particles were redispersed in toluene. Then the above wash and purification process was proceeded twice. The final precipitation was resuspended in *n*-hexane.

**First-Principle Calculations of  $\text{Cs}_3\text{Cu}_2\text{Cl}_5$ :** Density functional theory calculations were performed using the QuantumATK package. Atomic coordinates were first fully relaxed until the force on atoms is less than  $10^{-3}$  eV Å<sup>-1</sup> with the experimental cell parameters constrained. Generalized gradient approximation of PBE (Perdew–Burke–Ernzerhof) was used as the exchange–correlation potential. Brillouin zone was sampled with a  $4 \times 4 \times 6$  Monkhorst–Pack grid for the bulk structure, Fermi–Dirac occupation method with broadening of 300 K was used for the numerical accuracy. Electronic properties were calculated at the theory level of HSE06 hybrid functional, projector augmented-wave and norm-conserving pseudopotential were employed to calculate the electronic band structure and density of states, respectively, and

the kinetic energy cutoff for plane-wave basis was set to be 20 and 40 Hartree accordingly.

**Fabrication of Warm White Light-Emitting Diodes (WLEDs):** Red  $\text{CaAlSiN}_3\text{:Eu}^{2+}$  phosphors were added into equal amounts of transparent epoxy A and B to mix together, followed by the dropping on 290 nm commercial UV chips. The chip with red phosphors was then heated in an oven at 90 °C for 1 h for solidification. Then the as-prepared  $\text{Cs}_3\text{Cu}_2\text{Cl}_5\text{:SiO}_x$  NCs were dropped on the top of solid  $\text{CaAlSiN}_3\text{:Eu}^{2+}$  phosphors followed by a heating of the WLEDs on a hot plate at 50 °C for 10 min to remove the solvent.

**Measurement of WLEDs and White Communication:** The as-fabricated WLEDs were measured by a spectroradiometer system (PR670, Photo Research). The WLEDs were driven by a sourceceter (Keithley 2400) to measure the optical properties (EL spectra, CCT, CRI, DUV values and CIE color coordinates). The experimental setup is illustrated in Figure 6a, where the electrical AC signal, generated by an arbitrary waveform generator (Rigol DG4102), was combined with a 7.0 V DC bias via a bias-T (Mini-Circuits Bias-Tee ZFBT-6GW+), and the resultant signal was utilized to the fabricated WLEDs. In order to convert the optical signal into an electrical signal, a photodetector (PD) (DH-GDT-D020V) with a  $-3$  dB bandwidth of 10 MHz was employed, and the resultant electrical signal was sampled by a digital storage oscilloscope (DSO) (LeCroy WaveSurfer 432) which was further processed offline via MATLAB.

**Characterizations:** The crystal phases of the samples were characterized by XRD with Cu K $\alpha$  radiation (XRD-6100, SHIMADZU, Japan). The TEM images were measured using a transmission electron microscope (Libra 200 FE, Zeiss, Germany). Fourier Transform Infrared (FTIR) spectra were performed using KBr tablets with a Nicolet iS50 FT-IR Spectrometer (Thermo Fisher Scientific, Waltham, MA, USA). Absorption spectrum was recorded ranging from 300 to 800 nm by a UV–vis spectrophotometer (UV-3800, SHIMADZU, Japan) under room temperature. The XPS were performed on an Escalab 250 Xi. Photoluminescence (PL) spectroscopy and the data of PLQY were measured by a PL system (FLS1000, Edinburgh Instruments) that was capable of measuring PL and PLQYs with an integration sphere was employed in this work.

## Supporting Information

Supporting Information is available from the Wiley Online Library or from the author.

## Acknowledgements

S.Z. and C.C. contributed equally to this work. The revised funding is National Natural Science Foundation of China (Nos. 61904023, 11974063); Postdoctoral Science Foundation of China (No. 2019M653336); Natural Science Foundation of Chongqing (No. cstc2019jcyj-bshX0078); Innovation Program of Postdoctor of Chongqing (No. CQBX201803). The authors would like to thank Dr. Bin Zhang and Miss Chuanyao Yang at Analytical and Testing Center of Chongqing University for their assistance with TEM and PL analysis.

## Conflict of Interest

The authors declare no conflict of interest.

## Data Availability Statement

Research data are not shared.



## Keywords

Cs<sub>3</sub>Cu<sub>2</sub>Cl<sub>5</sub> nanocrystals, excellent stability, lead-free perovskites, silica coating, visible light communication

Received: February 11, 2021

Revised: March 25, 2021

Published online:

- [1] Q. A. Akkerman, G. Raino, M. V. Kovalenko, L. Manna, *Nat. Mater.* **2018**, 17, 394.
- [2] F. Liu, Y. Zhang, C. Ding, S. Kobayashi, T. Izuishi, N. Nakazawa, T. Toyoda, T. Ohta, S. Hayase, T. Minemoto, K. Yoshino, S. Dai, Q. Shen, *ACS Nano* **2017**, 11, 10373.
- [3] Z. Tan, J. Li, C. Zhang, Z. Li, Q. Hu, Z. Xiao, T. Kamiya, H. Hosono, G. Niu, E. Lifshitz, Y. Cheng, J. Tang, *Adv. Funct. Mater.* **2018**, 28, 1801131.
- [4] T. C. Jellicoe, J. M. Richter, H. F. Glass, M. Tabachnyk, R. Brady, S. E. Dutton, A. Rao, R. H. Friend, D. Credgington, N. C. Greenham, M. L. Böhm, *J. Am. Chem. Soc.* **2016**, 138, 2941.
- [5] H. Liang, F. Yuan, A. Johnston, C. Gao, H. Choubisa, Y. Gao, Y. K. Wang, L. K. Sagar, B. Sun, P. Li, G. Bappi, B. Chen, J. Li, Y. Wang, Y. Dong, D. Ma, Y. Gao, Y. Liu, M. Yuan, M. I. Saidaminov, S. Hoogland, Z. H. Lu, E. H. Sargent, *Adv. Sci.* **2020**, 7, 1903213.
- [6] Z. Ma, Z. Shi, C. Qin, M. Cui, D. Yang, X. Wang, L. Wang, X. Ji, X. Chen, J. Sun, D. Wu, Y. Zhang, X. J. Li, L. Zhang, C. Shan, *ACS Nano* **2020**, 14, 4475.
- [7] Z. Luo, Q. Li, L. Zhang, X. Wu, L. Tan, C. Zou, Y. Liu, Z. Quan, *Small* **2019**, 16, 1905226.
- [8] L. Lian, M. Zheng, W. Zhang, L. Yin, X. Du, P. Zhang, X. Zhang, J. Gao, D. Zhang, L. Gao, G. Niu, H. Song, R. Chen, X. Lan, J. Tang, J. Zhang, *Adv. Sci.* **2020**, 2000195.
- [9] J. Zhang, Y. Yang, H. Deng, U. Farooq, X. Yang, J. Khan, J. Tang, H. Song, *ACS Nano* **2017**, 11, 9294.
- [10] Z. Ma, Z. Shi, D. Yang, F. Zhang, S. Li, L. Wang, D. Wu, Y. Zhang, G. Na, L. Zhang, X. Li, Y. Zhang, C. Shan, *ACS Energy Lett.* **2019**, 5, 385.
- [11] M. Leng, Y. Yang, K. Zeng, Z. Chen, Z. Tan, S. Li, J. Li, B. Xu, D. Li, M. P. Hautzinger, Y. Fu, T. Zhai, L. Xu, G. Niu, S. Jin, J. Tang, *Adv. Funct. Mater.* **2018**, 28, 1704446.
- [12] M. Leng, Z. Chen, Y. Yang, Z. Li, K. Zeng, K. Li, G. Niu, Y. He, Q. Zhou, J. Tang, *Angew. Chem., Int. Ed.* **2016**, 55, 15012.
- [13] B. Yang, J. Chen, S. Yang, F. Hong, L. Sun, P. Han, T. Pullerits, W. Deng, K. Han, *Angew. Chem., Int. Ed.* **2018**, 57, 5359.
- [14] S. Zhao, Q. Mo, W. Cai, H. Wang, Z. Zang, *Photonics Res.* **2021**, 9, 187.
- [15] P. Cheng, L. Sun, L. Feng, S. Yang, Y. Yang, D. Zheng, Y. Zhao, Y. Sang, R. Zhang, D. Wei, W. Deng, K. Han, *Angew. Chem., Int. Ed.* **2019**, 131, 1.
- [16] P. Sebastia-Luna, J. Navarro-Alapont, M. Sessolo, F. Palazon, H. J. Bolink, *Chem. Mater.* **2019**, 31, 10205.
- [17] R. Zhang, X. Mao, D. Zheng, Y. Yang, S. Yang, K. Han, *Laser Photonics Rev.* **2020**, 14, 2000027.
- [18] L. Xie, B. Chen, F. Zhang, Z. Zhao, X. Wang, L. Shi, Y. Liu, L. Huang, R. Liu, B. Zou, Y. Wang, *Photonics Res.* **2020**, 8, 768.
- [19] Y. Wei, X. Deng, Z. Xie, X. Cai, S. Liang, P. A. Ma, Z. Hou, Z. Cheng, J. Lin, *Adv. Funct. Mater.* **2017**, 27, 1703535.
- [20] Y. Duan, C. Ezquerro, E. Serrano, E. Lalinde, J. García-Martínez, J. R. Berenguer, R. D. Costa, *Adv. Funct. Mater.* **2020**, 30, 2005401.
- [21] Z. J. Li, E. Hofman, J. Li, A. H. Davis, C. H. Tung, L. Z. Wu, W. Zheng, *Adv. Funct. Mater.* **2018**, 28, 1704288.
- [22] Q. Zhang, B. Wang, W. Zheng, L. Kong, Q. Wan, C. Zhang, Z. Li, X. Cao, M. Liu, L. Li, *Nat. Commun.* **2020**, 11, 31.
- [23] H. Hu, L. Wu, Y. Tan, Q. Zhong, M. Chen, Y. Qiu, D. Yang, B. Sun, Q. Zhang, Y. Yin, *J. Am. Chem. Soc.* **2018**, 140, 406.
- [24] W. Song, Y. Wang, B. Wang, Y. Yao, W. Wang, J. Wu, Q. Shen, W. Luo, Z. Zou, *Nano Res.* **2020**, 13, 795.
- [25] C. Sun, Y. Zhang, C. Ruan, C. Yin, X. Wang, Y. Wang, W. W. Yu, *Adv. Mater.* **2016**, 28, 10088.
- [26] H. Guan, S. Zhao, H. Wang, D. Yan, M. Wang, Z. Zang, *Nano Energy* **2020**, 67, 104279.
- [27] Z. Li, L. Kong, S. Huang, L. Li, *Angew. Chem., Int. Ed.* **2017**, 56, 8134.
- [28] Q. Zhong, M. Cao, H. Hu, D. Yang, M. Chen, P. Li, L. Wu, Q. Zhang, *ACS Nano* **2018**, 12, 8579.
- [29] Q. Mo, T. Shi, W. Cai, S. Zhao, D. Yan, J. Du, Z. Zang, *Photonics Res.* **2020**, 8, 1605.
- [30] Z. Hu, Z. Liu, Y. Bian, S. Li, X. Tang, J. Du, Z. Zang, M. Zhou, W. Hu, Y. Tian, Y. Leng, *Adv. Opt. Mater.* **2018**, 6, 1700997.
- [31] X. Tang, W. Chen, Z. Liu, J. Du, Z. Yao, Y. Huang, C. Chen, Z. Yang, T. Shi, W. Hu, Z. Zang, Y. Chen, Y. Leng, *Small* **2019**, 15, 1900484.
- [32] S. Huang, Z. Li, L. Kong, N. Zhu, A. Shan, L. Li, *J. Am. Chem. Soc.* **2016**, 138, 5749.
- [33] L. Lian, M. Zheng, P. Zhang, Z. Zheng, K. Du, W. Lei, J. Gao, G. Niu, D. Zhang, T. Zhai, S. Jin, J. Tang, X. Zhang, J. Zhang, *Chem. Mater.* **2020**, 32, 3462.
- [34] R. Rocanova, A. Yangui, G. Seo, T. D. Creason, Y. Wu, D. Y. Kim, M. H. Du, B. Saparov, *ACS Mater. Lett.* **2019**, 1, 459.
- [35] R. Rocanova, A. Yangui, H. Nhalil, H. Shi, M. H. Du, B. Saparov, *ACS Appl. Electron. Mater.* **2019**, 1, 269.
- [36] M. H. Du, *ACS Energy Lett.* **2020**, 5, 464.
- [37] S. Li, J. Luo, J. Liu, J. Tang, *J. Phys. Chem. Lett.* **2019**, 10, 1999.
- [38] Z. Ma, L. Wang, X. Ji, X. Chen, Z. Shi, *J. Phys. Chem. Lett.* **2020**, 11, 5517.
- [39] F. Zhang, Z. F. Shi, Z. Z. Ma, Y. Li, S. Li, D. Wu, T. T. Xu, X. J. Li, C. X. Shan, G. T. Du, *Nanoscale* **2018**, 10, 20131.
- [40] J. F. Liao, Y. F. Xu, X. D. Wang, H. Y. Chen, D. B. Kuang, *ACS Appl. Mater. Interfaces* **2018**, 10, 42301.
- [41] S. Zhao, Y. Zhang, Z. Zhang, *Chem. Commun.* **2020**, 56, 5811.
- [42] R. Lin, Q. Guo, Q. Zhu, Y. Zhu, W. Zheng, F. Huang, *Adv. Mater.* **2019**, 31, 1905079.
- [43] X. Zhao, G. Niu, J. Zhu, B. Yang, J. H. Yuan, S. Li, W. Gao, Q. Hu, L. Yin, K. H. Xue, E. Lifshitz, X. Miao, J. Tang, *J. Phys. Chem. Lett.* **2020**, 11, 1873.